Available online at www.sciencedirect.com
ScienceDirect
Journal of Power Sources 160 (2006) 684–687
JOURNAL OF POWER SOURCES
www.elsevier.com/locate/jpowsour

Electrode properties of melt-spun Mg–Ni–Nd amorphous alloys

L.J. Huang *, G.Y. Liang, Z.B. Sun, D.C. Wu

Department of Materials Physics, Science School, Xi'an Jiaotong University, Xi'an 710049, China

Received 5 November 2005; received in revised form 19 December 2005; accepted 21 December 2005
Available online 17 February 2006

Abstract

Amorphous and nanocrystalline Mg-based alloys $(Mg_{60}Ni_{25})_{100-x}Nd_x$ ($x = 2, 5, 10, 15$) were prepared by rapid solidification. The microstructure of the as-quenched ribbons was characterized by TEM, X-ray and electron diffraction. The electrode properties of these alloys were measured. The experimental results showed that the discharge capacities increased with increasing Nd atomic content and the optimum Nd content is between in 10–15 mol%. The highest discharge capacity reached more than 580 mAh g^{-1} at the discharge current densities of 50 mA g^{-1} for $(Mg_{60}Ni_{25})_{90}Nd_{10}$ samples. The nanocrystalline $(Mg_{60}Ni_{25})_{98}Nd_2$ alloy showed the lowest discharge capacity compared to the other Mg–Ni–Nd amorphous alloys. The alloy $(Mg_{60}Ni_{25})_{90}Nd_{10}$ displays the broadest discharge potential flat from 1.3 to 1.0 V. It was conformed that the increase of discharge capacities is not only a function of the sample composition but strongly influenced by the amorphous phase proportion in the alloys.

Keywords: Magnesium alloys; Melt-spun; Amorphous alloy; Electrode properties

1. Introduction

Magnesium and magnesium-based hydrogen storage alloys are promising energy conversion and storage materials because of their absorbability of hydrogen in large quantities, lower specific gravity, richer mineral resources, low material cost and so on. The Mg_2Ni compound has been the most intensively investigated and expected to have a bright future as an electrode material for the Ni–MH battery [1–4]. Furthermore, the effect of adding a third element to the Mg–Ni-based alloy on the discharge capacity has been investigated [5–8]. This previous result has shown that the discharge capacity of Mg–Ni-based ternary alloys produced by the mechanical alloying (MA) and rapidly solidified technique significantly depend on the species and amounts of the third element. In addition, the discharge capacities of these ternary alloys decrease gradually with increasing cycle numbers even in the low range of 10–20 cycles. The poor life cycle properties of Mg-based alloys are generally attributed to the poor dissociation ability of metallic Mg for hydrogen molecules and also to the formation of surface hydrides which hinder the further transport of hydrogen into the matrix [9–11].

In the present work, we used the melt-spun technique for sample preparation with the aim of avoiding the significant degradation of life cycle properties which was recognized in many previous studies on Mg–Ni-based alloys [5–11]. Since the Mg_2Ni crystalline compound is well known to possess high hydrogen storage capacity, we have chosen amorphous alloys with the compositions near Mg_2Ni. Consequently, we must add other element, which can increase the glass forming ability of Mg–Ni-based alloys and also act as an efficient catalyst for dissociating H_2 molecules and transferring the H atoms to the surrounding Mg_2Ni matrix. In this studies so far, it has been found that an amorphous single phase can be obtained by the addition of a small amount of La, Y or Nd to the Mg_2Ni alloy and the Nd addition is more effective to improve the life cycle properties of amorphous Mg–Ni-based alloys as compared with the other two elements. This study intends to present the electrode properties of the rapidly solidified $(Mg_{60}Ni_{25})_{100-x}Nd_x$ ($x = 2, 5, 10, 15$) amorphous alloy and to investigate the effectiveness of the rapid solidification process on the development of high discharge capacity materials.

2. Experimental

$(Mg_{60}Ni_{25})_{100-x}Nd_x$ ($x = 2, 5, 10, 15$) alloy ingots were prepared by induction melting a mixture of pure Nd metal and

* Corresponding author. Tel.: +86 29 82673545; fax: +86 29 82665079.
E-mail addresses: newboy66@126.com (L.J. Huang), gyliang@mail.xjtu.edu.cn (G.Y. Liang).

0378-7753/$ – see front matter © 2006 Elsevier B.V. All rights reserved.
doi:10.1016/j.jpowsour.2005.12.072

a Mg–Ni alloy in a vacuum furnace under the protection of argon gas. Based on the low melting point and the high vapor pressure of Mg, a special melting technique, that is positive pressure protection and repeated melting, has to be taken to prevent massive Mg evaporation and ensure composition homogeneity during master alloy ingot preparation. The amorphous or nanocrystalline ribbons were produced by a single roller melt-spun technique (copper quenching disc with a diameter of 250 mm and surface velocity of about 39 ms^{-1}) in an argon atmosphere of 400 mbar. The ribbons were about 2 mm wide and 20 μm thick. The microstructure of the as-quenched ribbons was characterized by transmission electron microscopy (Philips CM200 operated at 200 kV) and by X-ray (using Cu Kα radiation) and electron diffraction.

In electrochemical measurement, the amorphous alloy ribbons were pulverized in a mortar and then mixed with nickel powder and PTFE in the ratio 85:5:10, respectively. This composite electrode material was pressed on a Ni grid to form the negative electrode. The positive electrode was made of Ni-oxyhydroxide/dihydroxide. The alkaline solution was 6 mol l^{-1} KOH containing 20 g l^{-1} LiOH. The specimens were charged at 100 mA g^{-1} for 12 h and discharged at 50 mA g^{-1}. The discharged cut-off potential was set to 0.8 V between the two electrodes. The resting time between the charge and discharge was 1 h. Hydrogen charging of specimens (negative electrode) was carried out electrolytically under galvanostatic conditions in 6 mol l^{-1} KOH electrolyte containing 20 g l^{-1} LiOH at room temperature and a cathodic current densities $i = 1$ mA cm^{-2} for 3 h. The hydrogen content was measured from the increase in mass after hydrogenation by a microbalance (Perkin-Elmer TGS2) with an accuracy of 0.1 μg.

3. Result and discussion

Fig. 1 presents the X-ray diffraction patterns of the as-quenched $(Mg_{60}Ni_{25})_{98}Nd_2$, $(Mg_{60}Ni_{25})_{95}Nd_5$, $(Mg_{60}Ni_{25})_{90}Nd_{10}$ and $Mg_{60}Ni_{25}Nd_{15}$. It is seen that the as-quenched

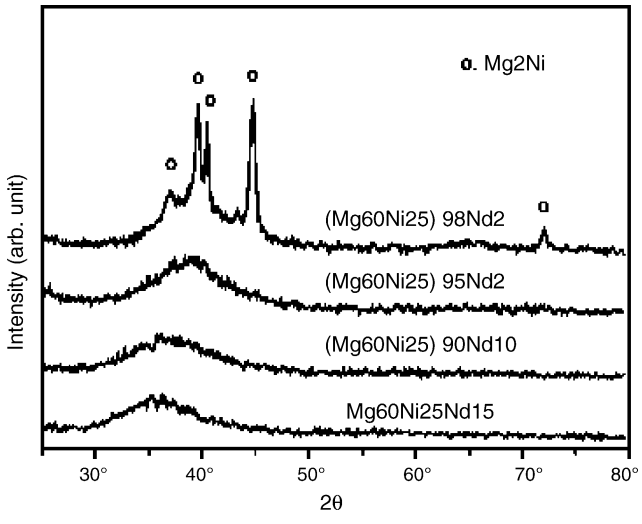

Fig. 1. X-ray diffraction patterns (Cu Kα) of as-quenched alloys.

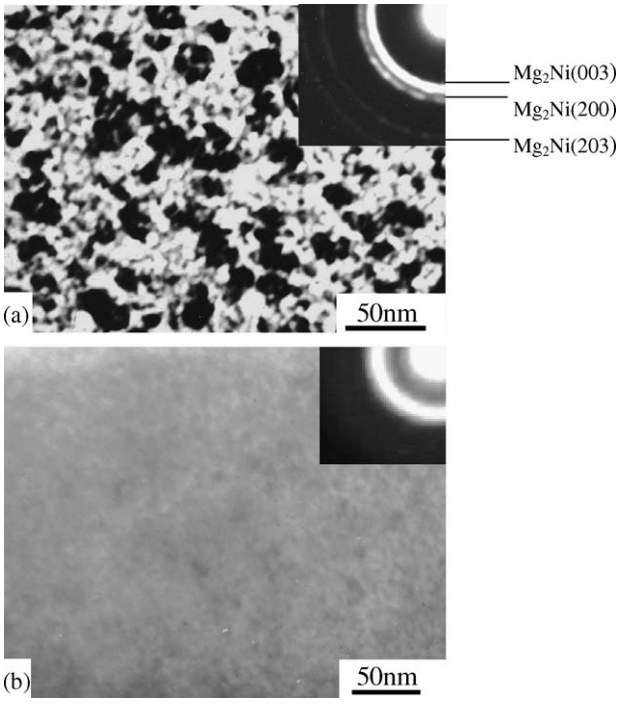

Fig. 2. TEM image and electron diffraction pattern of as-quenched. $(Mg_{60}Ni_{25})_{98}Nd_2$ (a) and $(Mg_{60}Ni_{25})_{95}Nd_5$ (b).

$(Mg_{60}Ni_{25})_{98}Nd_2$ alloy reveals a nanocrystalline structure with some amorphous phases. When the neodymium content exceeds 5 mol%, the alloys $(Mg_{60}Ni_{25})_{95}Nd_5$, $(Mg_{60}Ni_{25})_{90}Nd_{10}$ and $Mg_{60}Ni_{25}Nd_{15}$ all show only a broad and diffuse peak, namely the featureless appearance is typical of amorphous structure. It is also seen that the typical amorphous peaks get smooth and low with the neodymium content increasing, which implies more uniform of elements in the amorphous structure.

The TEM image of as-quenched $(Mg_{60}Ni_{25})_{98}Nd_2$ alloy is shown in Fig. 2a. It is found that the hexagonal Mg_2Ni structure was detected from the electron diffraction pattern, and a wide diffraction ring typical of amorphous structure is in the XRD pattern. It was presumed that the nanocrystalline Mg_2Ni was embedded in the amorphous matrix. The TEM image and electron diffraction pattern of as-quenched $(Mg_{60}Ni_{25})_{95}Nd_5$ alloy are showed in Fig. 2b. It is found that a uniform amorphous structure was obtained.

Fig. 3 shows the variation of the discharge capacity of the different samples: $(Mg_{60}Ni_{25})_{98}Nd_2$, $(Mg_{60}Ni_{25})_{95}Nd_5$, $(Mg_{60}Ni_{25})_{90}Nd_{10}$ and $Mg_{60}Ni_{25}Nd_{15}$, versus the number of cycles. It can be observed that whatever the cycle number is $(Mg_{60}Ni_{25})_{90}Nd_{10}$ has the highest capacity and $(Mg_{60}Ni_{25})_{98}Nd_2$ has the lowest one. For each composition, with increasing the cycle numbers the discharge capacity to reach a maximum after three or four cycles, and then decreases for upper cycle numbers. The curves of the discharge capacity turn to smooth after 10 cycles. The largest discharge capacity of samples reached 80.2 mAh g^{-1} for 2 mol% Nd, 262.6 mAh g^{-1} for 5 mol% Nd, 580.5 mAh g^{-1} for 10 mol% Nd and 541.8 mAh g^{-1} for 15 mol% Nd.

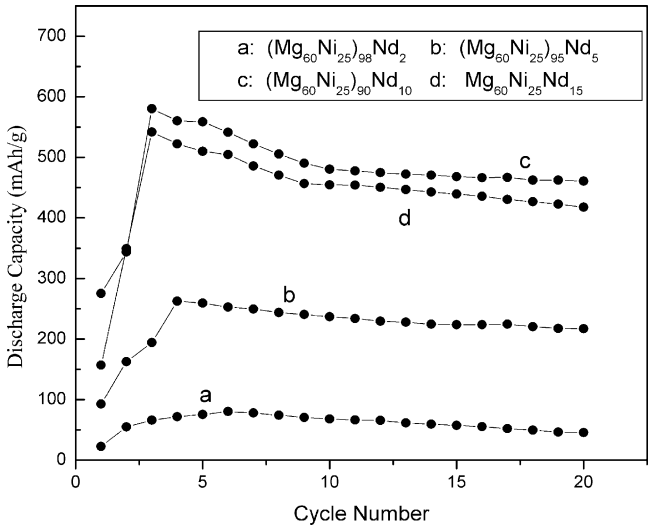

Fig. 3. Variation of the discharge capacity vs. the cycle number for the different samples.

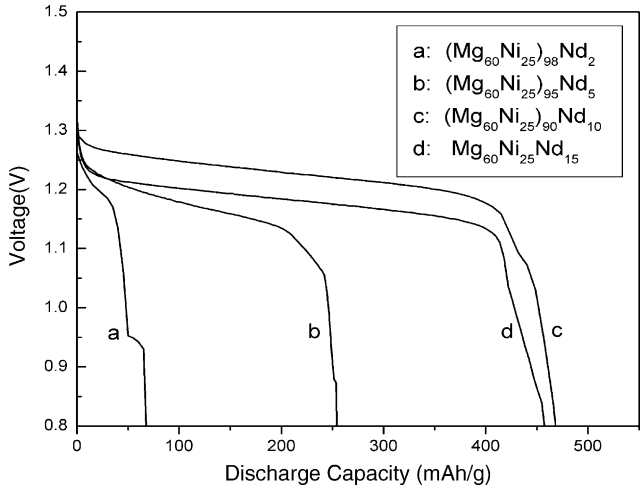

Fig. 5. Relationship of voltage and the discharge capacities (at the 10th cycle).

Fig. 4 gives the variation, as function of the Nd atomic content, of the maximum discharge capacity (C_{max}) and the discharge capacity after 20 cycles (C_{20}). After 20 cycles, the discharge capacity C_{20} reaches 57% of the discharge capacity C_{max} for 2 mol% Nd alloy, 83% for 5 mol% alloy, 80% for 10 mol% alloy and 77% for 15 mol% alloy.

From above results, it is considered that the increase of discharge capacities is not only a function of the sample composition but strongly influenced by the amorphous phase proportion in the alloyed material. As the content of Nd increases, the diffraction peak at about 40° shifts to lower angle (Fig. 1), this suggests the disordered degree of their structures increased [12]. That would enhance hydrogen diffusivity and solubility in amorphous and disordered structures, associated with the wide energy distribution of the available sites for hydrogen in the glassy structure as well as avoiding the long-range diffusion of hydrogen through an already formed hydride. At the same time, the $Mg(OH)_2$ hydroxide forms on the grain boundaries during the electrochemical reaction, which obstructs the diffusion of hydrogen atoms in the grain. Because the thickness of the hydroxide layer increases with increasing the cycle number, the discharge capacity decreases with increasing the cycle number.

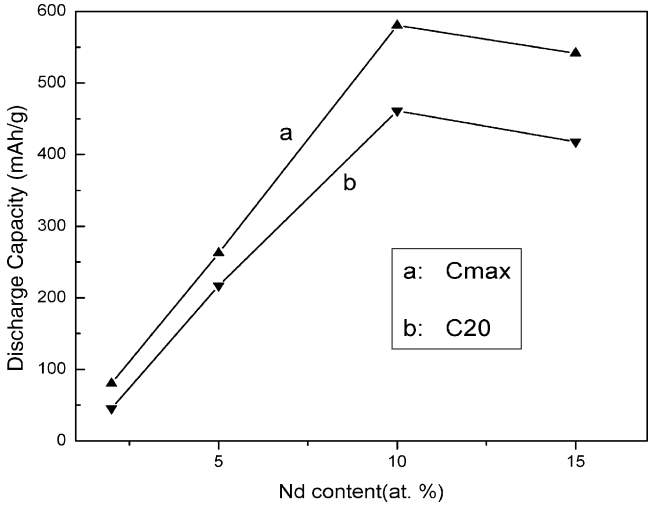

Fig. 4. Variation of the discharge capacity (maximum capacity and after 20 cycles) as a function of the Nd atomic content.

The relationship of discharge potentials (voltage) and the discharge capacities (at the 10th cycle) is shown in Fig. 5. It is seen that there is a discharge potential flat from 1.3 to 1.0 V for each alloy with variation of the discharge capacity which denotes a range of discharge capacity that the alloy can be used. It is found that the discharge capacities of the discharge potential flats have reached more than 400 mAh g^{-1} for alloys $Mg_{60}Ni_{25}Nd_{15}$ and $(Mg_{60}Ni_{25})_{90}Nd_{10}$. However, the discharge capacity of the discharge potential flat of $(Mg_{60}Ni_{25})_{98}Nd_2$ alloy is only 50 mAh g^{-1}. It is also important to point out that the discharge capacity is significantly dependent on the composition and microstructure of the electrode materials.

The rate of hydrogen absorption of $(Mg_{60}Ni_{25})_{90}Nd_{10}$ amorphous alloys at room temperature is plotted in Fig. 6. In this figure, another hydrogenation kinetic curve has been attached, which is obtained in Tony Spassov's previous study at similar charging conditions [13]. Tony Spassov et al. showed that the best hydrogenation properties so far were found in the nanocrystalline/amorphous $Mg_{75}Ni_{20}Mm_5$ (Mm = Ce, La-rich mischmetal) alloy, which possesses maximum hydrogen capacity 4.0 wt.% H . Both of kinetic curves of hydrogenation show an initial fast hydrogen absorption stage. Subsequently, the hydrogen content is saturated at longer hydrogenation times. It is seen that the $(Mg_{60}Ni_{25})_{10}Nd_{10}$ sample displays the maximum hydrogen absorption content, which is up to 4.2 wt.% although its initial ratio of hydrogen absorption is lower in the beginning of 60 min.

The discharge capacities and hydrogenation kinetics of all as-quenched amorphous and nanocrystalline/amorphous Mg–Ni–Nd alloys studied are superior to those of conventional polycrystalline materials with similar compositions.

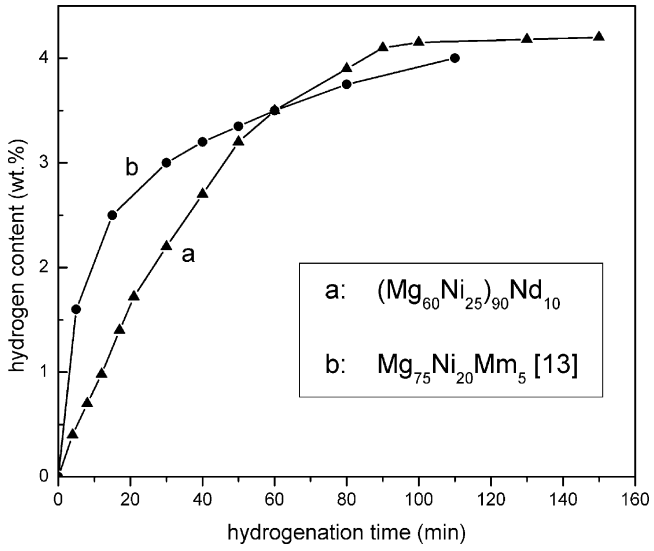

Fig. 6. Rate of hydrogen absorption for as-quenched $(Mg_{60}Ni_{25})_{10}Nd_{10}$ and $Mg_{75}Ni_{20}Mm_5$ alloys.

The improved electrode properties can be explained with the enhanced hydrogen diffusivity and solubility in amorphous and nanocrystalline microstructures. In the case of the amorphous $(Mg_{60}Ni_{25})_{90}Nd_{10}$ and $Mg_{60}Ni_{25}Nd_{15}$ alloys consist of a significant proportion of amorphous phase leading to an easier access of hydrogen to the hydriding regions, avoiding the long-range diffusion of hydrogen through an already formed hydride, which is often the slowest stage of H-absorption.

According to the result of Orimo and Fujii [14] reported, hydrogen concentrations in three nanometer-scale regions and the maximum hydrogen concentrations of the three regions have been experimentally determined to be 0.3 wt.% H in the grain region of Mg_2Ni, 4.0 wt.% H in the grain boundary and 2.2 wt.% H in the amorphous region. It revealed that the hydrides mainly exist in grain-boundary region and the amorphous phase region. It is necessary to be mentioned that the melt-spun amorphous $(Mg_{60}Ni_{25})_{90}Nd_{10}$ alloy in the present study contains substantially larger amount of amorphous phase compared to the nanocrystalline $Mg_{75}Ni_{20}Mm_5$ alloy studied by Tony Spassov et al. [13]. Another possible reason for the higher H-capacity and discharge capacity of the $(Mg_{60}Ni_{25})_{90}Nd_{10}$ could be the higher rare earth(Nd) content(10 at.%) in this alloy as compared to the $Mg_{75}Ni_{20}Mm_5$ alloy. Rare earth is known to work as catalysts for the hydrogenations of Mg. Tony Spassov and Uweköster [15] observed an improvement in the hydrogenation kinetics of $Mg_{63}Ni_{30}Y_7$ alloy due to the catalytic effect of Yttrium.

For practical use of the Mg-based amorphous alloy as both an electrode material and a hydrogen storage material, we have to improve the composition more in detail, particularly in order to attain the equilibrium state more quickly at which the highest absorbed hydrogen amount is obtained.

4. Conclusions

The electrode properties of the rapidly solidified Mg–Ni–Nd amorphous alloys were examined. The results obtained are summarized as follows:

1. The single amorphous phase was obtained in the melt-spun $(Mg_{60}Ni_{25})_{95}Nd_5$, $(Mg_{60}Ni_{25})_{90}Nd_{10}$ and $Mg_{60}Ni_{25}Nd_{15}$ ribbons.
2. In the cyclic life measurements, the discharge capacities increased with increasing Nd atomic content and the optimum Nd content is between 10 and 15 mol%. The highest discharge capacity reached more than 580 mAh g^{-1} at the discharge current densities of 50 mA g^{-1} for $(Mg_{60}Ni_{25})_{90}Nd_{10}$ samples and the discharge capacity reaches 80% of the maximum discharge capacity after 20 cycles.
3. There is a discharge potential flat from 1.3 to 1.0 V for each alloy with variation of the discharge capacity. The discharge capacities of the discharge potential flat have reached more than 400 mAh g^{-1} for alloys $Mg_{60}Ni_{25}Nd_{15}$ and $(Mg_{60}Ni_{25})_{90}Nd_{10}$. However, the discharge capacity of the discharge potential flat of $(Mg_{60}Ni_{25})_{98}Nd_2$ alloy is only 50 mAh g^{-1}.
4. The amorphous $(Mg_{60}Ni_{25})_{90}Nd_{10}$ alloy shows the best hydrogen absorption properties so far and its absorption capacity up to 4.2 wt.% H.

Acknowledgements

This study was supported by the Doctoral Foundation of Xi'an Jiaotong University (Grant No. DFXJTU-200516) and National Natural Science Foundation of China (Grant No. 50371066).

References

[1] H.Y. Lee, N.H. Goo, W.T. Jeong, K.S. Lee, J. Alloys Compd. 313 (2000) 258.
[2] L. Sun, G.X. Wang, H.K. Liu, D.H. Bradhurst, S.X. Dou, Electrochem. Solid-State Lett. 3 (3) (2000) 121.
[3] M. Abdellaoui, S. Mokbli, F. Cuevas, M. Latroche, A. Percheron-Guégan, H. Zarrouk, J. Alloys Compd. 356/357 (2003) 557.
[4] A.A. Mohamad, N.S. Mohamed, Y. Alias, A.K. Arof, J. Power Sources 115 (2003) 161.
[5] T.-W. Hong, Y.-J. Kim, J. Alloys Compd. 330–332 (2002) 584.
[6] S. -Ichi, H.-Y. Kim, H. Kimnra, A. Inoue, Y. Arata, J. Alloys Compd. 347 (2002) 239.
[7] J. Yin, K. Tanaka, Mater. Trans. 43 (7) (2002) 1732.
[8] M. Savyak, S. Hirnyj, H.-D. Bauer, M. Uhlemann, J. Eckert, L. Schultz, A. Gebert, J. Alloys Compd. 364 (2004) 229.
[9] L.-B. Wang, Y.-H. Tang, Y.-J. Wang, Q.-D. Li, H.-N. Song, H.-B. Yang, J. Alloys Compd. 336 (2002) 297.
[10] J.-J. Jiang, M. Gasik, J. Power Sources 89 (1) (2000) 117.
[11] J. Yin, K. Tanaka, N. Tanaka, Mater. Trans. 43 (3) (2002) 417.
[12] T.C. Hufnagel, Nature Mater. 3 (2004) 666.
[13] T. Spassov, V. Rangelova, N. Neykov, J. Alloys Compd. 334 (2002) 219.
[14] S. Orimo, H. Fujii, Appl. Phys. A 72 (2001) 167.
[15] T. Spassov, Uweköster, J. Alloys Compd. 287 (1999) 43.